Environmental Science: Atmospheres

ROYAL SOCIETY OF CHEMISTRY

PAPER

View Article Online
View Journal | View Issue

Cite this: *Environ. Sci.: Atmos.*, 2021, **1**, 508

Atmospheric inputs of volcanic iron around Heard and McDonald Islands, Southern ocean†

Morgane M. G. Perron, *[a] Bernadette C. Proemse,[a] Michal Strzelec,[a] Melanie Gault-Ringold[b] and Andrew R. Bowie[ab]

Atmospheric deposition of iron to anemic waters in the Southern Ocean (SO) can relieve marine phytoplankton growth limitation. The northern Kerguelen plateau, in the iron-limited Indian sector of the SO, hosts vast annual spring blooms of marine phytoplankton, evidencing seasonal iron supply mechanisms. This study reports the first atmospheric measurements of iron concentration and solubility near and downwind of the volcanically active islands of Heard and McDonald Islands (HIMI) on the Kerguelen plateau. Using a combination of atmospheric tracers (radon and black carbon), air-mass back-trajectories, and trace metal ratios in aerosols, we detected emission from Heard Island in aerosols up to 500 km downwind from HIMI. The latter emissions were characterized by enrichment in molybdenum (Mo, ~100 to 3000-fold), chromium (Cr) and nickel (Ni) (both ~5 to 40-fold) in aerosols compared to Heard Island basaltic rocks. This phenomena reflects the greater volatility of Mo, Cr and Ni compared to the lithogenic reference trace metal aluminum (Al) under volcanic eruption atmospheric conditions. Our study highlights that volcanic emissions from Heard Island's main volcano, Big Ben, should be considered an additional source of atmospheric Fe supply to marine ecosystems near and downstream of the Kerguelen plateau, alongside other volcanic clusters in the Southern Hemisphere.

Received 5th July 2021
Accepted 23rd August 2021

DOI: 10.1039/d1ea00054c

rsc.li/esatmospheres

Environmental significance

Southern ocean marine productivity participates in regulating the global climate through mitigating atmospheric CO_2 content. The Heard and McDonald Islands (HIMI) are two volcanically-active islands on the Northern Kerguelen plateau, in the Southern Indian ocean. There, seasonal blooms of phytoplankton evidence local iron (Fe) supply mechanisms to seawater which remain poorly understood. This study shows that volcanic emissions from Heard Island resulted in increased atmospheric loading of bioavailable Fe around and up to 500 km downwind from HIMI. Volcanic emission can therefore represent a significant source of Fe to open ocean anaemic ecosystems. Such source is currently poorly or unaccounted for in biogeochemical models, likely causing models to underestimate marine productivity over the Southern ocean and its feedbacks on climate.

1. Introduction

The Southern Ocean (SO, south of 30°S) is a key regulator of global climate, and responsible for up to 43% of the anthropogenic CO_2 uptake, and 75% of the Earth's excess heat taken up globally by the oceans between 1861 and 2005.[1] The SO is also the Earth's largest High Nutrient Low Chlorophyll (HNLC) marine region, where primary productivity is drastically limited by sub-nanomolar concentrations of the trace element iron (Fe), ultimately impacting the SO capacity to buffer climate change.[2] On and downstream of the Kerguelen plateau, in the Indian sector of the SO, spring and early summer marine phytoplankton blooms are annually observed by satellite imagery and shipboard observations.[3,4] Such increases in oceanic primary productivity have been shown to result from enhanced supply of bioavailable Fe to this marine region, including but not limited to direct inputs from the Kerguelen plateau.[3,5–8]

The Australian Territory of Heard and McDonald Islands (HIMI) are two volcanically-active islands on the southern end of the northern Kerguelen plateau.[9,10] During the HEOBI ('Heard Earth Ocean Biosphere Interactions') campaign, despite phytoplankton biomass being low, strong ecosystem growth was measured,[11] consistent with high Fe supply. Local Fe supply mechanisms to surrounding seawaters were previously attributed, in part, to glacial outflows from Heard Island,[12,13] sediment resuspension and upwelling[4] south of HIMI, or underwater hydrothermalism near McDonald Island.[5] While atmospheric Fe deposition from the volcanically-active HIMI seems like a plausible candidate as a source of bioavailable Fe to seawater, the latter has not been investigated to date. Eastwards

[a]*Institute for Marine and Antarctic Studies, University of Tasmania, Battery Point, Tasmania, Australia. E-mail: morgane.perron@utas.edu.au*

[b]*Antarctic Climate and Ecosystems CRC, University of Tasmania, Battery Point, Tasmania, Australia*

† Electronic supplementary information (ESI) available. See DOI: 10.1039/d1ea00054c

transport by SO westerly winds[13] of dust and volcanic gases from McDonald Island as well as ash erupted from Heard Island's volcano Big Ben[10] may result in the fertilisation of Fe-depleted marine ecosystems on and downwind of the Kerguelen plateau. Large volcanic eruptions have been shown to temporarily relieve Fe-limitation on phytoplankton growth in HNLC marine areas.[13–16] Modelling studies suggest that substantial contribution from currently unaccounted for aeolian sources such as volcanic eruptions may hinder accurate representations of the atmospheric labile Fe loading over the Southern ocean.[17] Ash deposition also supplies other metals such as molybdenum (Mo), nickel (Ni) and chromium (Cr),[13,14,16] and the atmospheric enrichment of these elements can serve as a fingerprint for volcanic emissions over remote oceanic areas.

While recent studies have described the underwater biogeochemistry of Fe around HIMI and off the Kerguelen plateau,[3,5,6,18] Fe-laden volcanic and dust emissions from the two islands remain unquantified.

This study reports first measurements of the total concentration and labile fraction of Fe in aerosols collected in the vicinity and downwind of HIMI when volcanic activity was visually witnessed on both islands. Atmospheric measurements (black carbon, radon) and air-mass trajectory modeling provided insights into the origin and transport pathway of Fe-containing aerosols along the voyage track between Australia and HIMI and around the volcanic islands. Metal ratios in Heard Island seabed rocks served as a reference to assess the contribution of volcanic emissions from the islands to aerosol loading during the campaign.

2. Material and methods

2.1 Sampling location

The Heard Earth Ocean Biosphere Interactions "HEOBI" voyage (GEOTRACES process study GIpr05) took place in the austral summer 2016 on board the Australian Marine National Facility R.V. Investigator. The remote islands of HIMI are a ~10 days transit (4100 km) away from Fremantle in Western Australia, and 1700 km north of Antarctica. The voyage consisted of a 30 days circumnavigation of the two islands which are only 43 km apart yet show very contrasting geology. Heard Island is about one million years old, large (368 km^2) and mostly glaciated and its rock composition is dominated by basalt. McDonald Island is much smaller (2.5 km^2), about 100 000 years old and totally ice-free, and is predominantly composed of phonolitic rocks.[9,10] During the campaign, signs of volcanic activity were visually witnessed on both islands in the form of lava flow on the flanks and smoke off the volcanic crater of Heard Island's volcano, Big Ben, and gas plumes (fumaroles) on McDonald Island (https://blog.csiro.au/big-ben-erupts/).

2.2 Ship-board aerosol sampling

Thirteen aerosol samples (A1–A13) were collected on acid-washed 47 mm circular Whatman 41 cellulose filters.[19] Air was drawn into a dedicated aerosol sampling laboratory through a 18 m a.s.l polished stainless-steel inlet tube running along the ship's foremast and leading into a high efficiency particulate air-filtered laminar flow hood using antistatic and conductive silicone tubing.[20] Aerosol sampling was only conducted under head winds (270–90° relative to the ship's bow) using an automated sector sampling switch to prevent contamination from the ship's exhaust. During the voyage, wind speeds ranged between 10 and 40 knots, avoiding any risk of sample contamination from stagnant air masses. Upon recovery, filters were stored in double plastic-bagged Petri dishes in the freezer. Procedural blank filters were acid washed filters mounted on the unpowered sampler for 5 min and were used to correct for trace metal blanks. Aerosol collection was previously detailed in full in Perron *et al.* (2020).[20] Additional information on aerosol sample collection is available in the ESI Table S1.†

2.3 Definition of soluble, labile and total Fe content in aerosol samples

Laboratory work was carried out following GEOTRACES 'Cookbook' procedures[21] and using ultra-high purity Baseline (Seastar chemicals®) and in-house distilled chemicals.

The three-step leaching protocol applied to aerosols was described in Perron *et al.* (2020).[20] Briefly, soluble Fe (S_{Fe}) in aerosols was extracted using an instantaneous flow-through leaching method using ultra-high purity water. The same filter was then soaked in 1.1 mol L^{-1} ammonium acetate (pH = 4.7) for one hour. The sum of Fe concentrations measured in the first two leaches is referred to as labile Fe (L_{Fe}). Finally, 12 h-long heat-assisted HF/HNO_3 digestion provided satisfactory recovery of all target elements on the remaining filter. Table S2† summarises the digestion recoveries (using the Arizona Test Dust (ATD) standard reference material) obtained during this study ($n = 1$), during the protocol assessment study ($n = 3$),[19] as well as the average recovery based on all digestions undertaken in our laboratory to date ($n = 7$). Concentrations of Fe in the leaches and digestion solution were analysed by sector field inductively coupled plasma-mass spectrometry (SF-ICP-MS, Thermo Fisher Scientific ELEMENT 2).[20] The sum of Fe concentrations measured following each step of the protocol defines the total Fe (T_{Fe}) content in aerosols. Concentrations are expressed in nanogram per cubic meter (ng m^{-3}) of air filtered after appropriate blank correction. Iron fractional solubility, $L_{Fe\%}$, is calculated as the percentage of L_{Fe}/T_{Fe} in each sample, using L_{Fe} rather than S_{Fe} as an estimate for bioavailable Fe in aerosols.[20]

2.4 Prevailing atmospheric influence on aerosols

Atmospheric circulation corresponding to each sample is traced back using a combination of air-mass back-trajectories and atmospheric measurements of radon (^{222}Rn) and black carbon (BC) concentrations.

The publicly available Hybrid Single-Particle Lagrangian Integrated Trajectory model (HYSPLIT) from the NOAA Air Resource Laboratory[22] is used to compute five-day back-trajectories for all dominant air masses arriving at each sample mid-point and recovery dates and locations (Fig. S3†).

Large uncertainty is associated with the use of HYSPLIT to track air-mass transport over more than a few days and from a moving sampling platform like a ship. In addition to HYSPLIT analysis, atmospheric ^{222}Rn concentrations were continuously measured along the voyage track using an independent 700 L two-filter radon detector connected to the same air inlet as the aerosol sampling system. Radon concentrations exceeding the SO baseline value of 50 mBq m^{-3} highlighted recent terrestrial inputs to the atmosphere.[23] In this study, continental influence may originate from Australia or from upwind Southern ocean islands such as the Kerguelen, Crozet or HIMI.

Atmospheric BC concentrations were monitored throughout the campaign using a multiangle absorption photometer (Thermo Fisher Scientific). Data acquisition was limited to the same 270–90° wind sector as operational aerosol sampling to exclude measurements of the ship's exhaust. In the remote and largely pristine environment of the Southern ocean, positive anomalies in atmospheric BC concentration indicate natural carbonaceous emissions from large fires closer to Australia or from volcanic emissions from HIMI.

2.5 Rock sampling and analysis

Seabed rocks were collected around HIMI using a rock dredge. Samples include two debris avalanches (R1 and R3) collapsed from the island's volcano, Big Ben, and 4 sea knolls (R2–R6). Visual characterisation of the rocks confirmed the basanite (basalt) nature of samples R1 and R2 (R3) rocks, reflecting the geological composition of Heard Island. Samples R4–R6 were identified as phonolitic rocks from the McDonald Island. Details of sampling dates, locations and visual descriptions are summarized in Table S3.†

Rock samples (~200 mg) were crushed and digested in open Teflon vessels at 120 °C on a hotplate successively using several H_2O_2 + HNO_3, HCl + HNO_3/HF, and HNO_3 + $HClO_4$ mixtures. Rock digests were analysed for trace metal composition by SF-ICP-MS (Element 2, Thermo Fisher Scientific, Inc.). This data is used as a local volcanic reference in the calculus of elemental ratios and enrichment factors (EF).

2.6 Metal ratios and enrichment factors

Enrichment factors (EF) are used to further discriminate between dominant sources of trace metals in aerosols.[18,24] Enrichment factors are calculated, following eqn (1), as the total concentration ratio of trace metal (T_x) to aluminum (T_{Al}), T_x/T_{Al}, in aerosols compared to the average of the same ratio measured in a chosen reference (a) in HIMI rocks or (b) in the average upper continental crust (UCC):[25]

$$EF_{x\text{-reference}} = \frac{T_x/T_{Al}(\text{aerosols})}{T_x/T_{Al}(\text{reference})} \quad (1)$$

Volcanic emissions are identified when volatile metals such as Cr, Mo, Ni (but also Cd, As, Cu, Zn…*etc.*, depending on the volcanic rock composition) contained in aerosols are enriched, up to several orders of magnitude, compared to the primary volcanic rock or lava.[26–28] In this study, a significant enrichment is indicated by EF > 10.[24]

3. Results and discussion

3.1 Source tracing in HEOBI aerosol samples

Table 1 shows the main atmospheric influence on individual aerosols collected during HEOBI according to the combined analysis of HYSPLIT air-mass back-trajectories and atmospheric measurements of ^{222}Rn and BC concentrations.

Overall, characteristic open ocean radon measurements (^{222}Rn < 100 mBq m^{-3}) and HYSPLIT transport model (Fig. S3†) suggested that the sampling locations of aerosols A3 to A12 predominantly receive oceanic air-masses. The lowest ^{222}Rn concentrations (58.9–61.0 mBq m^{-3}) of the voyage, reaching values typical of SO westerly winds ^{222}Rn signature (~50 mBq m^{-3} (ref. 23)), was measured during collection of A3, A4 and

Table 1 Main atmospheric influence in aerosols based on the analysis of individual HYSPLIT air-mass back-trajectories, measurement of atmospheric radon (^{222}Rn, mBq m^{-3}) and black carbon (BC, μg m^{-3}) concentrations over each sampling period and the total concentration ratio of vanadium-to-manganese (T_V/T_{Mn}) in aerosols. Aerosol ID and estimated distance (km, orientation) to Heard Island is also displayed[a]

Atmospheric influence		Aerosol ID	Distance to Heard Island	T_V/T_{Mn}	HYSPLIT	^{222}Rn	BC
Oceanic influence	(1) HIMI	HEOBI-A7	137.1 (W)	0.36	W, Southern Ocean (SO)	90.3	0.02
		HEOBI-A8	71.4 (W)	0.34	W, SO	84.6	0.05
		HEOBI-A10	57.9 (W)	0.17	W, HIMI	83.5	0.15
		HEOBI-A9	15.9 (SE)	0.25	W, SO – Kerguelen	86.7	0.04
		HEOBI-A11	80.2 (NE)	0.61	NW, HIMI	92.6	0.06
		HEOBI-A6	201.9 (NE)	0.14	W, HIMI	83.1	0.02
		HEOBI-A5	504.5 (NE)	0.19	W, SO long-range	86.3	0.00
	(2) Transit voyage "pristine SO air"	HEOBI-A12	1130.9 (NE)	<BL	W, SO long-range	61.0	0.01
		HEOBI-A4	1685.6 (NE)	0.10	W, SO	58.9	0.00
		HEOBI-A3	2789.2 (NE)	<BL	W, SO long-range	58.9	0.02
	(3) Anthropogenic from Australia	HEOBI-A2	3303.6 (NE)	5.52	Indian ocean/Australia	189	0.02
		HEOBI-A13	3455.0 (NE)	3.09	Great Australian Bight	413	0.00
		HEOBI-A1	3782.6 (NE)	6.36	Great Australian Bight	2458	0.87

[a] <BL: concentration below the filter blank.

A12. Therefore, the latter samples primarily contain "pristine" air issued from long-range (>10 days) aeolian transport over the SO. Higher atmospheric ^{222}Rn concentrations (83.1–92.6 mBq m^{-3}) during the sampling period of aerosols A5 to A11, while circumnavigating HIMI, highlight small terrestrial inputs in those samples from subaerial emissions on the Kerguelen plateau. Contrastingly, aerosols A1, A2 and A13, collected closer to Australia, show both air-mass back-trajectories and atmospheric ^{222}Rn concentrations indicative of a coastal land influence (^{222}Rn = 189–413 mBq m^{-3}) in A2 and A13 and a clear continental fingerprint (^{222}Rn = 2458 mBq m^{-3}) in A1.

High vanadium-to-manganese (T_V/T_{Mn}) ratios (T_V/T_{Mn} > 1) has been postulated to reveal the presence of anthropogenic emission in aerosols.[29] Amongst all aerosols collected during the voyage, only A1, A2 and A13, collected close to western Australia, displayed T_V/T_{Mn} ratios exceeding 1 (3.1–6.4, Table 1). This observation further supports the presence of continental aerosols in these samples, specifically anthropogenic emissions from industries, traffic and power production from Australia. We therefore endorse Sedwick *et al.* (2007)[29] hypothesis that T_V/T_{Mn} > 1 can serve as a tracer for human-derived aeolian emissions in open ocean aerosols.

Atmospheric BC can be emitted by combustion processes from anthropogenic activities, natural fires or volcanoes.[30] A background atmospheric BC concentration of 0–0.02 μg m^{-3}, indicating the absence of combustion emissions in aerosols, is recorded along most of the voyage track except aerosols A8 to A11 and aerosol A1. Aerosols A8 to A11 are associated with BC concentrations between 0.04–0.15 μg m^{-3}. The samples were collected less than 100 km away from HIMI, following a thermal anomaly (28th of January) detected on Heard Island[31] by middle infrared radiation observation from MODIS satellite.[32] Such a sign of early volcanic activity was confirmed on the 30th and 31st of January as campaign's participants visually witnessed fumaroles and lava flow on the McDonald and Heard Islands (https://volcano.si.edu/volcano.cfm?vn=234010), respectively. As no other combustion source is present in this remote region, measurements of atmospheric BC 2 to 10-fold greater than background concentrations over the sampling period of A8–A11 (Table 1) reveal that the samples likely comprise volcanic emissions originating from HIMI. The highest BC loading of 0.87 μg m^{-3} corresponds to the sampling period of A1 (Table 1) which coincides with large fire events in the Waroona-Yarloop (Western Australia).[33] Hypothetical contamination from the ship's exhaust is excluded due to the thorough selection of head-winds (270–90°) and comparative observations of BC.

3.2 Atmospheric Fe measurements

Measurements of the total concentration (T_{Fe}) and labile fraction (L_{Fe}) of Fe in HEOBI aerosols are shown in Table 2.

Total Fe loading in aerosols ranged from 0.4 to 32.7 ng m^{-3}. Aerosols A1, A2 and A13, which include continental emissions from Australia (T_V/T_{Mn} > 1), contained Fe concentrations between 1.1 and 32.7 ng m^{-3}, which falls within the range of atmospheric T_{Fe} concentrations previously reported over Australian coastal waters (0.8–102.9 ng m^{-3})[34] and in subantarctic waters south east of Tasmania (5–17 ng m^{-3}).[35] Samples collected over the transit periods between Australia and HIMI (A3, A4, A12), as well as A5, contained the smallest T_{Fe} contents (0.4–1.2 ng m^{-3}, Table 1), which compare well with pristine SO air Fe loadings (0.04–5.8 ng m^{-3}) measured at the Cape Grim SO baseline air station, Australia[36] but is smaller than the T_{Fe} range of 6.1–38 ng m^{-3} reported along a similar transect in the SO.[37] Such small Fe concentrations reflect the gradual loss of Fe-laden particles by gravitational settling during long-range atmospheric transport.[38,39] At closer proximity (<200 km) to HIMI (A6–A11), we observed a tendency for increased T_{Fe} concentration (0.7–3.0 ng m^{-3}) in aerosols compared to open SO samples, reaching similar atmospheric T_{Fe} concentrations as measured downwind of Australia[34] and in the Southern Indian Ocean off Madagascar (2.8–8.6 ng m^{-3}).[40] This provided evidence that local atmospheric inputs of Fe, from islands on the Kerguelen plateau (including HIMI), can be detected in aerosols collected as far as 200 km away from HIMI.

Aerosols A1, A2 and A13 presented high Fe solubilities ($L_{Fe\%}$), between 8% and 24%, compared to mineral Fe solubility values

Table 2 Total Fe concentration (T_{Fe}, ng m^{-3}), labile Fe fraction (L_{Fe}, %), soluble-to-labile Fe ratio (S_{Fe}/L_{Fe}, %) and T_{Fe}/T_{Al} ratio in each aerosol sample collected during HEOBI. Enrichment factors for Fe are presented relative to both the average UCC[25] ($EF_{Fe\text{-}UCC}$) and HI rock composition (this study, $EF_{Fe\text{-}HI}$). Samples are ordered by increasing distance (km) to the west (W) and to the east (E) of Heard Island (HI)

Sample	Distance to HI (km)	T_{Fe} (ng m^{-3})	$L_{Fe\%}$ (%)	S_{Fe}/L_{Fe} (%)	T_{Fe}/T_{Al}	$EF_{Fe\text{-}UCC}$	$EF_{Fe\text{-}HI}$
HEOBI-A7	137 (W)	2.0	8	62	3.4	7.8	1.8
HEOBI-A8	71 (W)	0.9	10	73	1.9	4.3	1.0
HEOBI-A10	58 (W)	3.0	7	46	1.8	4.1	0.9
HEOBI-A9	16 (SE)	1.4	15	67	0.8	1.8	0.4
HEOBI-A11	80 (NE)	0.7	22	57	1.6	3.7	0.8
HEOBI-A6	202 (NE)	2.5	12	44	1.8	4.1	0.9
HEOBI-A5	504 (NE)	0.8	19	73	2.5	5.7	1.3
HEOBI-A12	1131 (NE)	0.8	52	34	0.3	0.7	0.2
HEOBI-A4	1686 (NE)	1.2	11	100	2.2	5.0	1.1
HEOBI-A3	2789 (NE)	0.4	54	54	1.0	2.4	0.5
HEOBI-A2	3304 (NE)	2.1	24	89	0.5	1.1	0.3
HEOBI-A13	3455 (NE)	1.1	16	63	0.4	0.9	0.2
HEOBI-A1	3783 (NE)	32.7	8	100	0.5	1.2	0.3

($L_{Fe\%}$ < 4%) commonly reported downwind from dust sources.[41,42] These same samples also contained a large fraction of water-soluble Fe (S_{Fe}/L_{Fe} > 63%), indicating a high degree of atmospheric processing.[43] Thus, anthropogenic emission detected (T_V/T_{Mn} > 1) in A1, A2 and A13 likely resulted in enhanced Fe solubilities in the samples through proton-promoted dissolution of Fe in the presence of acidic compounds (*e.g.* sulfur and nitrogen oxides) emitted by combustion processes.[34,44,45] Enhanced Fe solubility in A1 and A13 may also result from ligand-mediated Fe dissolution in the presence oxalate-laden pyrogenic particles. Indeed, significant concentration of biomass burning tracer, levoglucosan, of 4 ng m^{-3} and 714 ng m^{-3} in A13 and A1, respectively, was previously reported in those samples[46] and is consistent with the detection of BC in A1 in this study. Aerosols collected during the transit period (A3, A4 and A12) and A5 presented the highest $L_{Fe\%}$ solubilities (11–54%), with similar values to the range of aerosol solubility reported at the Cape Grim SO baseline station (0.5–56%).[36] High Fe solubility over 10% in aerosols collected over the SO was previously attributed to solubility-enhancing processes undergone by aerosols during long-range atmospheric transport.[43,47,48] Greater Fe solubility (~82%) was reported in rainwater samples collected on the Kerguelen Island, which was attributed to the small size of particles following long-range atmospheric transport over the Southern ocean.[49] Compared to the transit period, $L_{Fe\%}$ near HIMI (A6–A11) decreased to 7–22% (Table 2) and was associated with smaller degree of atmospheric processing (44% < S_{Fe}/L_{Fe} < 73%). This feature reflects fresh input of less soluble aeolian Fe, likely from HIMI islands, in A6 to A11. Generally, aerosols collected closer to McDonald Island (A7, A8, A10) contained less soluble Fe ($L_{Fe\%}$ < 10%) compared to aerosols collected around Heard (A6, A9, A11) where the $L_{Fe\%}$ fraction ranged from 12% to 22%. Unique atmospheric conditions created by Big Ben volcanic eruption, *i.e.* high temperature and acidic compounds emission (SO_2, HCl, HF),[14,50] could explain higher Fe solubility in samples collected closer to Heard Island compared to dust-dominated aerosols collected near the ice-free McDonald Island. The analysis of EF_{Fe} is necessary to further discriminate the origin of mineral Fe in aerosols collected during the HEOBI campaign.

3.3 Heard Island emission fingerprint in HIMI aerosols

Trace metal measurements in seabed rocks (Table 3) collected in the vicinity of HIMI (R1–R6) compare well with previously reported values.[9] Very contrasting total Fe-to-Al concentration ratios are observed between Heard Island volcanic rocks (1.3 < T_{Fe}/T_{Al} < 2.3) and the average ratios measured in McDonald Island rocks (T_{Fe}/T_{Al} = 0.43) and in the average upper continental crust (UCC, T_{Fe}/T_{Al} = 0.44).[25] Therefore, the clear Fe enrichment (58.2–85.4 mg g^{-1}) and depletion in Al (average of 40.2 mg g^{-1}) in Heard Island rocks can be used to track the fingerprint of Heard Island atmospheric emission in aerosols in this study.

In all aerosols collected during the HEOBI campaign, enrichment factor of Fe relative to the average upper continental crust ($EF_{Fe\text{-}UCC}$) is predominantly of lithogenic origin, as suggested by $EF_{Fe\text{-}UCC}$ < 10, rather than an anthropogenic origin. However, we observed variations in the concentration ratio of total Fe-to-Al, T_{Fe}/T_{Al} (Table 2 and Fig. 1), according to aerosol sampling locations, suggesting the existence of distinct mineral sources along the voyage track. In the following section, T_{Fe}/T_{Al} ratios in aerosols are compared to the same ratio in Heard Island rocks and in the average UCC in order to discriminate dominant sources of mineral Fe in each sample (Fig. 1).

Aerosols collected the closest to Australia (A1, A2, A13) present T_{Fe}/T_{Al} ratios between 0.4 and 0.5, which is comparable to the same ratio in the average UCC ($T_{Fe}/T_{Al,\ UCC}$ = 0.44 (ref. 25)). Resulting $EF_{Fe\text{-}UCC}$ (0.9–1.2) values close to 1 confirm that, while A1, A2 and A13 contain anthropogenic combustion particles (T_V/T_{Mn} > 1 and enhanced L_{Fe} fraction), total Fe loading in these samples is dominated by emissions from Australian dust sources.

Although aerosol A12 is suggested to receive air-masses issued from long-range transport over the SO, high Al content in this sample results in a T_{Fe}/T_{Al} ratio of 0.3, slightly smaller than that of the average UCC ($EF_{Fe\text{-}UCC}$ = 0.7). It can therefore be postulated that A12 receives a unique (Al-rich) atmospheric influence transported from the west; for example, dust from southern Africa. Other aeolian samples collected over the Southern ocean (A3–A11, excluding A9) all showed T_{Fe}/T_{Al} exceeding 1 (Table 2), reflecting the gravitational settling of Al-rich crustal material in favour of smaller combustion-like particles rich in Fe with increasing distance from emission source. The highest T_{Fe}/T_{Al} ratios (>2.2) were found in samples A4, A5 and A7 and slightly exceeded the same ratio measured in basanite rocks (2.0) from Heard Island. Sample A4 was collected about 1686 km east (downwind) of Heard Island, thus it seems

Table 3 Measurements of Fe concentration (T_{Fe}, ng m^{-3}), Fe-to-Al ratio (T_{Fe}/T_{Al}) and enrichment factor in Fe compared to the upper continental crust ($EF_{Fe\text{-}UCC}$[25]) in the rock samples dredged around HIMI

Rock samples		Geology	T_{Fe} [mg g^{-1}]	T_{Al} [mg g^{-1}]	T_{Fe}/T_{Al}	$EF_{Fe\text{-}UCC}$
Heard Island	R1	Basanite	80.0	32.0	2.5	5.7
	R2	Basanite	90.9	44.4	2.0	4.7
	Average		85.44	38.2	2.3	5.2
	R3	Basalt	58.2	44.2	1.3	3.0
McDonald	R4	Phonolite	26.3	77.4	0.34	0.8
	R5	Phonolite	28.4	88.1	0.32	0.7
	R6	Phonolite	42.3	69.6	0.6	1.4
	Average		32.3	78.4	0.43	1.0

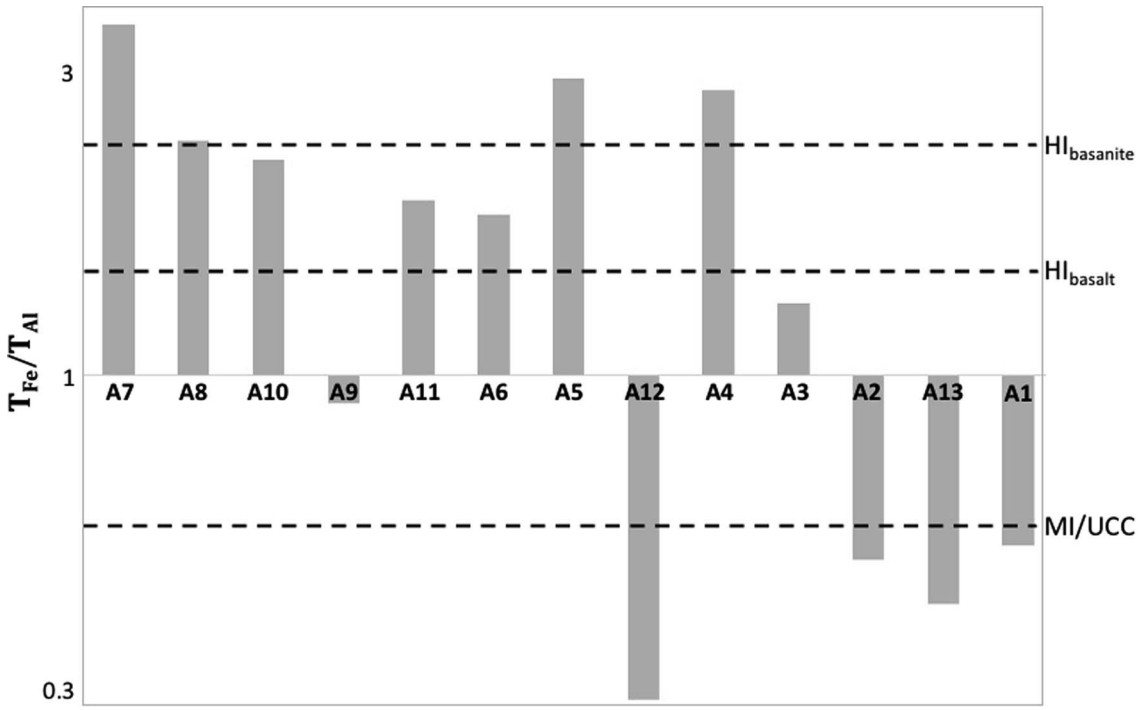

Fig. 1 Total concentration ratio of Fe-to-Al, T_{Fe}/T_{Al}, in aerosols collected during the HEOBI campaign. Horizontal dashed lines represent the same ratio measured in the averaged upper continental crust (UCC from McLennan *et al.*, (2001)[24]) and in rocks dredged near Heard Island (HI) and McDonald Island (MI) for comparison. A log scale view was chosen for better visualization of the different T_{Fe}/T_{Al} ratios between samples.

unlikely that this sample primarily receive aeolian emissions from the island. The absence of recent lithogenic input (^{222}Rn = 58.9 mBq m^{-3}) and the extremely high degree of atmospheric processing (S_{Fe}/L_{Fe} = 100%) measured in this sample indicate that A4 content is dominated by well-mixed air-masses delivered *via* long-range eastwards atmospheric transport over the SO. On the other hand, aerosols A5 and A7, sampled about 500 km downwind and 100 km upwind of HIMI, both show signs of a fresh crustal input (increase in ^{222}Rn > 86 mBq m^{-3}, Table 1). Iron enrichment in A5 and A7 compared to other aerosols collected in the vicinity of HIMI highlight that another source of Fe contributes to aerosol composition of the latter samples alongside local mineral Fe input from the islands. Well-mixed long-range transported aerosols (enriched in Fe compared to Al) are plausible candidate to explain T_{Fe}/T_{Al} > 2.2 in A5 and A7.

Other aerosols collected around HIMI (excluding A9) display Fe-to-Al ratios between 1.6 and 1.9, remarkably similar to the same ratio (T_{Fe}/T_{Al} = 1.8) in volcanic rocks dredged near Heard Island when averaging both basaltic and basanite rocks (Table 3). This observation emphasises a significant influence from Heard Island emissions to the atmosphere (A5–A11) around and downwind of the islands. Due to the quasi-complete ice cover on Heard Island, such emissions are likely to originate from the volcanic eruption of Big Ben during the voyage. Volcanic conditions from Big Ben eruption are consistent with enhanced Fe solubility measured in A5–A11 (7% < $L_{Fe\%}$ < 22%, Table 2) compared to commonly reported mineral Fe solubility as explained in paragraph 3.2. Despite a close proximity to Heard Island, sample A9 shows very unique patterns. High Al content in this sample results in a low Fe-to-Al ratio of 0.8 compared to the reference volcanic rocks ($EF_{Fe\text{-}HI}$ = 0.4). HYSPLIT analysis suggest that A9 mainly receives air-masses originating from long-range aeolian transport which flowed over the ice-free Kerguelen Islands. Soil from the Kerguelen Islands was previously reported to have a Fe-to-Al ratio of 0.54,[51] similar to the average T_{Fe}/T_{Al} UCC value of 0.44.[25] Since the ratio of Fe-to-Al in A9 falls between the reported values for Heard Island and the average UCC or Kerguelen Island ratios, we suggest that this sample may be influenced by a mixture of air-masses from both origins. This hypothesis may also explain the diluted (low) atmospheric BC concentration measured in this sample. Another hypothesis would be that a quasi-equal contribution of Heard Island (T_{Fe}/T_{Al} = 1.8) and McDonald Island (T_{Fe}/T_{Al} = 0.43) emissions is comprised in A9.

3.4 Volcanic aerosol emission around HIMI

Most trace metals analysed in aerosols along the HEOBI voyage track show highly variable concentrations and EFs. Yet, a clear enrichment in Cr, Ni and Mo can be noticed in aerosols A5–A11 (Fig. 2) collected around the volcanic islands that is not found in any other samples.

Chromium and Ni exist in small quantities in the Earth's upper crust, however, these metals are highly enriched (2.6 and 3.5 times, respectively) in the Earth mantle[25] which is brought to the surface during volcanic eruptions. Molybdenum exists

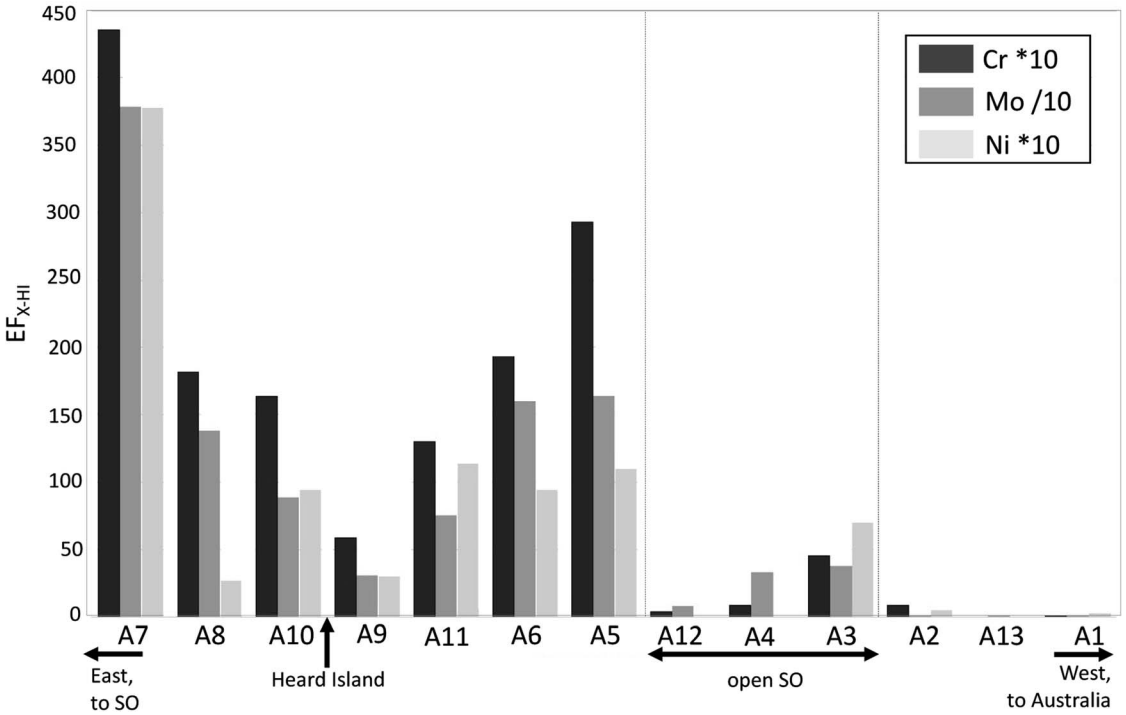

Fig. 2 Enrichment factors of Cr, Mo, and Ni-relative to Heard Island average rock measurements in aerosols collected during the HEOBI campaign. Samples are ordered by decreasing distance to the west and increasing distance to the east of Heard Island. For better visualisation, EFs were divided by 10 for Mo and multiplied by 10 for Cr and Ni.

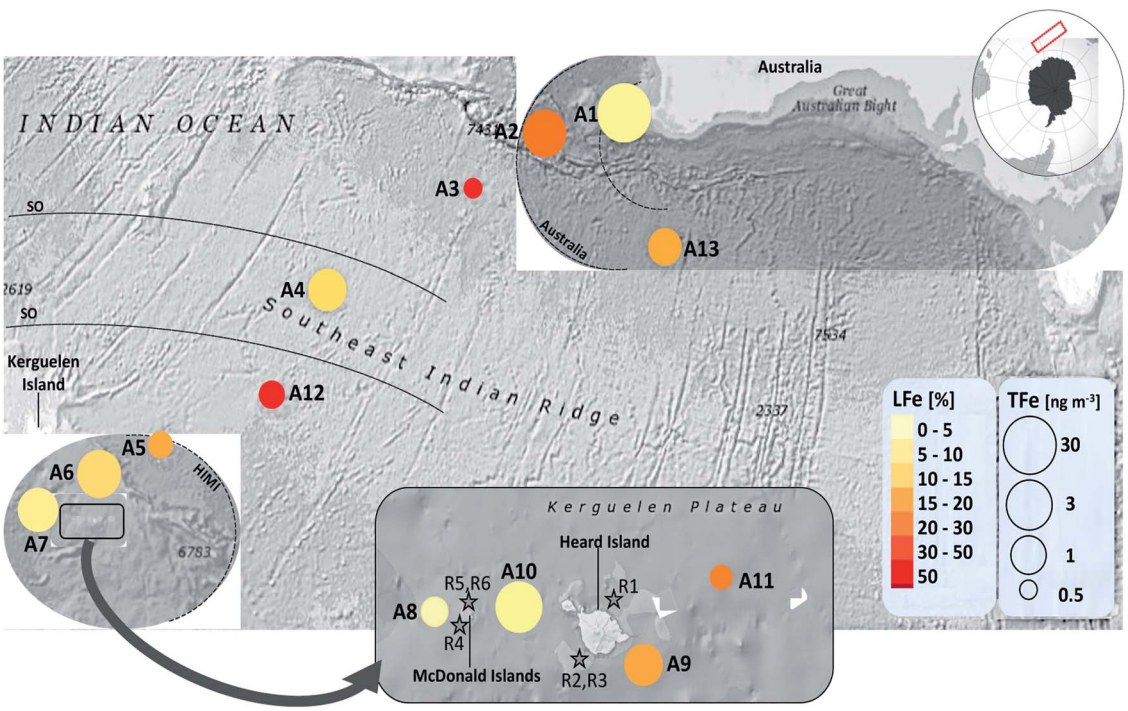

Fig. 3 Measurement of the total concentration, T_{Fe} (ng m^{-3}, point size), and labile fraction, $L_{Fe\%}$ (%, colour scale), of Fe in aerosols collected during the HEOBI campaign. Aerosol samples A1–A13 are represented by their mid-sampling location. $L_{Fe\%}$ equals to 54 and 52% for A3 and A12, respectively. Samples A8–A11 were collected whilst the research vessel circumnavigated both islands. Rock sample (R_x) locations are indicated with grey stars. The dashed black lines and grey shading illustrate dominant aeolian influence found in aerosols, either volcanic emissions from Heard Island volcano, air mass issued from long-range transport over the SO or Australian dust and anthropogenic combustion particles.

equally in the upper crust and the Earth's mantle, although this element is more volatile than other refractory metals such as Al used to calculate EFs,[28] as are Cr and Ni to a lesser extent. This higher volatility result in enrichments of a factor 2 for Cr and Ni and a factor 3–4 for Mo commonly reported in volcanic aerosols and gases compared to the primordial volcanic rock composition.[26–28] This signature may therefore be used to track volcanic emissions to the atmosphere.

High $EF_{x\text{-}HI}$ in Cr (6 to 44), Ni (3 to 38) and Mo (306 to 3791) were found in aerosols A5-A11 compared to Heard Island average rock composition (Fig. 2). The latter samples also presented similar T_{Fe}/T_{Al} signature to that of Heard Island's basaltic rocks, which greatly differ from McDonald island phonolitic rock characteristics (Table 3 and Fig. 1). In the absence of atmospheric sources of Cr, Ni and Mo in the remote SO, we conclude that latter metal enrichments in samples A5–A11 provide evidence of the impact of volcanic emissions from Heard Island lava eruption (rather than McDonald island fumaroles) on the atmospheric composition up to 500 km downwind of the island. Sample A9 showed smaller enrichment in Cr, Mo and Ni than other aerosols collected around HIMI (Fig. 2), which is consistent with the hypothesis that this sample contains mixed air-masses and includes influences from the Kerguelen Island and McDonald Island (Section 3.3), rather than HIMI alone.

Our observations highlight that volcanic emissions from Big Ben eruption on Heard Island do influence atmospheric composition about 200 km around (A6–A11) and up to 500 km downwind (A5) to the volcano (Tables 1 and 2). Fig. 3 summarizes dominant aeolian influences and the associated atmospheric Fe measurements in samples collected along the ship's track during the HEOBI campaign. Volcanic plumes will transport nutrients and metals, but also heat and acidic compounds (SO_2, HCl, HF)[14,50] which influence atmospheric Fe composition and the subsequent supply of labile Fe following atmospheric deposition, to marine ecosystems down the aeolian pathway. According to the time of the year atmospheric deposition occurs, this mechanism may lead to ocean fertilisation and increase in marine productivity.

4. Conclusions

This study presents Fe measurements in aerosols collected around the Southern ocean's remote and active volcanic islands of Heard and McDonald (HIMI). Increased atmospheric Fe loadings (average $T_{Fe} = 1.8$ ng m^{-3}) near HIMI compared to Southern ocean aerosol concentrations (average $T_{Fe} = 0.8$ ng m^{-3}), and no Fe enrichment in those aerosols (EF_{Fe} close to 1) compared to the averaged upper Earth crust, are evidence of the existence of a local supply of mineral Fe on the southern part of the northern Kerguelen plateau. Such fresh atmospheric input of Fe is associated with a labile Fe ($L_{Fe\%}$) fraction between 7% and 22%, higher than poor Fe solubility (<4%) generally reported in mineral aerosols but lower than L_{Fe} measurements in samples influenced by long-range aeolian transport following extensive atmospheric processing. Mineral Fe input around HIMI was identified as originating from Heard island emissions to the atmosphere as suggested by similar T_{Fe}/T_{Al} ratios in aerosols compared to seabed rocks characteristic of Heard Island basalt and basanite. Atmospheric emissions from Heard Island were further characterised as volcanic ash from the eruption of Big Ben volcano based on distinctive enrichments in volcanic volatile metals, including Cr, Ni (by a factor 2) and Mo (by a factor 3–4), measured in aerosols up to 500 km downwind to the island. Such observation show that Cr, Mo and Ni can be used in future studies as atmospheric tracers of Heard Island volcanic eruptions to the atmosphere over this part of the Southern ocean.

More generally, our study raises awareness on the importance of the impact of volcanic emissions on atmospheric composition and on the subsequent deposition of bioavailable nutrients (including Fe) to remote oceanic areas such as the Southern ocean. Ito and co-workers (2020) previously highlighted that aerosol measurements around HIMI were largely (80%) associated with aeolian sources that are currently unaccounted for in model parametrizations.[17] Our study shows that unique atmospheric conditions created by Big Ben volcanic eruption, *i.e.* high temperature and acidic compounds emission (SO_2, HCl, HF),[14,50] are likely responsible for enhanced Fe solubility measured in samples collected closer to Heard Island. It is therefore essential to include volcanic emissions in modelling representations of atmospheric Fe emissions over parts of the ocean, including the Southern ocean and around the Pacific ring of fire.

During the HEOBI campaign, while phytoplankton biomass was reported to be low, rapid ecosystem growth was measured[11] which is consistent with high Fe supply. Despite the small magnitude of Big Ben eruption during the campaign, we suggest that input of new volcanic Fe to the ocean around and downwind of HIMI may have helped sustain the observed rapid ecosystem growth. Further study is necessary to better understand the role of larger volcanic eruptions in fertilizing or in bringing toxic elements to aquatic ecosystems; this source should also be an inherent part of biogeochemical models, especially at a regional scale.

Author contributions

A. R. B. was responsible for project conceptualization, funding acquisition, fieldwork investigation, resources and supervision. M. M. G. P. was responsible for analysis, data curation and original draft writing. All authors were responsible for data interpretation and validation and reviewing and editing the manuscript.

Conflicts of interest

There are no conflicts to declare.

Acknowledgements

The authors wish to thank the CSIRO Marine National Facility (MNF) for ship-time on RV Investigator voyage IN2016_V01, with excellent help from the crew, support personnel, and data

managers. We also thank Prof Zanna Chase, Dr Jodi Fox and the MNF crew for shipboard rock sampling and identification as well as interesting idea inputs to this manuscript. All data and samples acquired on the voyage will be made publicly available in both IMAS and CSIRO Data Portals. This work was supported by an Australian Research Council Future Fellowship (FT130100037 to A. R. B.), the Australian Antarctic Science Grants Program (AAS4338 to Mike Coffin) and through the Antarctic Climate and Ecosystems Cooperative Research Centre (ACE CRC).

References

1 T. L. Frölicher, J. L. Sarmiento, D. J. Paynter, J. P. Dunne, J. P. Krasting and M. Winton, *J. Clim.*, 2015, **28**, 862–886.
2 P. W. Boyd, A. J. Watson, C. S. Law, E. R. Abraham, T. W. Trull, R. Murdoch, D. C. E. Bakker, A. R. Bowie, K. O. Buesseler, H. Chang, M. Charette, P. L. Croot, K. Downing, R. Frew, M. Gall, M. Hadfield, J. Hall, M. Harvey, G. Jameson, J. LaRoche, M. Liddicoat, R. Ling, M. T. Maldonado, R. M. M. Mckay, S. Nodder, S. Pickmere, R. Pridmore, S. Rintoul, K. Safi, P. Sutton, R. F. Strzepek, K. Tanneberger, S. Turner, A. Waite and J. Zeldis, *Nature*, 2000, **407**, 695–702.
3 S. Blain, B. Quéguiner, L. Armand, S. Belviso, B. Bombled, L. Bopp, A. R. Bowie, C. Brunet, C. Brussaard, F. Carlotti, U. Christaki, A. Corbière, I. Durand, F. Ebersbach, J. L. Fuda, N. Garcia, L. Gerringa, B. Griffiths, C. Guigue, C. Guillerm, S. Jacquet, C. Jeandel, P. Laan, D. Lefèvre, C. Lo Monaco, A. Malits, J. Mosseri, I. Obernosterer, Y. H. Park, M. Picheral, P. Pondaven, T. Remenyi, V. Sandroni, G. Sarthou, N. Savoye, L. Scouarnec, M. Souhaut, D. Thuiller, K. Timmermans, T. Trull, J. Uitz, P. Van Beek, M. Veldhuis, D. Vincent, E. Viollier, L. Vong and T. Wagener, *Nature*, 2007, **446**, 1070–1074.
4 C. Schallenberg, S. Bestley, A. Klocker, T. W. Trull, D. M. Davies, M. Gault-Ringold, R. Eriksen, N. P. Roden, S. G. Sander, M. Sumner, A. T. Townsend, P. van der Merwe, K. Westwood, K. Wuttig and A. R. Bowie, *J. Geophys. Res.: Oceans*, 2018, **123**, 5986–6003.
5 T. M. Holmes, K. Wuttig, Z. Chase, P. van der Merwe, A. T. Townsend, C. Schallenberg, M. Tonnard and A. R. Bowie, *Mar. Chem.*, 2019, **211**, 1–14.
6 A. R. Bowie, P. Van Der Merwe, F. Quéroué, T. Trull, M. Fourquez, F. Planchon, G. Sarthou, F. Chever, A. T. Townsend, I. Obernosterer, J. B. Sallée and S. Blain, *Biogeosciences*, 2015, **12**, 4421–4445.
7 F. Quéroué, G. Sarthou, H. F. Planquette, E. Bucciarelli, F. Chever, P. Van Der Merwe, D. Lannuzel, A. T. Townsend, M. Cheize, S. Blain, F. D'Ovidio and A. R. Bowie, *Biogeosciences*, 2015, **12**, 3869–3883.
8 F. Chever, G. Sarthou, E. Bucciarelli, S. Blain and A. R. Bowie, *Biogeosciences*, 2010, **7**, 455–468.
9 J. Barling, S. L. Goldstein and I. A. Nicholls, *J. Petrol.*, 1993, **35**, 1017–1053.
10 P. G. Quilty and G. Wheller, *Pap. & Proc. R. Soc. Tasmania*, 2000, **133**, DOI: 10.26749/rstpp.133.2.1.
11 B. Wojtasiewicz, T. W. Trull, L. Clementson, D. M. Davies, N. L. Patten, C. Schallenberg and N. J. Hardman-Mountford, *Front. Mar. Sci.*, 2013, **6**, DOI: 10.3389/fmars.2019.00531.
12 K. Kiernan and A. McConnell, *Polar Rec.*, 2002, **38**, 297–308.
13 M. G. Weinbauer, B. Guinot, C. Migon, F. Malfatti and X. Mari, *J. Plankton Res.*, 2017, **39**, 187–198.
14 S. Duggen, N. Olgun, P. Croot, L. Hoffmann, H. Dietze, P. Delmelle and C. Teschner, *Biogeosciences*, 2010, **7**, 827–844.
15 E. P. Achterberg, C. M. Moore, S. A. Henson, S. Steigenberger, A. Stohl, S. Eckhardt, L. C. Avendano, M. Cassidy, D. Hembury, J. K. Klar, M. I. Lucas, A. I. MacEy, C. M. Marsay and T. J. Ryan-Keogh, *Geophys. Res. Lett.*, 2013, **40**, 921–926.
16 J. Olsson, S. L. S. Stipp, K. N. Dalby and S. R. Gislason, *Geochim. Cosmochim. Acta*, 2013, **123**, 134–149.
17 A. Ito, M. M. G. Perron, B. C. Proemse, M. Strzelec, M. Gault-Ringold, P. W. Boyd and A. R. Bowie, *Prog. Earth Planet. Sci.*, 2020, **7**, DOI: 10.1186/s40645-020-00357-9.
18 P. van der Merwe, K. Wuttig, T. Holmes, T. W. Trull, Z. Chase, A. T. Townsend, K. Goemann and A. R. Bowie, *Front. Mar. Sci.*, 2019, **6**, 1–20.
19 P. L. Morton, W. M. Landing, S.-C. Hsu, A. Milne, A. M. Aguilar-Islas, A. R. Baker, A. R. Bowie, C. S. Buck, Y. Gao, S. Gichuki, M. G. Hastings, M. Hatta, A. M. Johansen, R. Losno, C. Mead, M. D. Patey, G. Swarr, A. Vandermark and L. M. Zamora, *Limnol. Oceanogr.*, 2013, **11**, 62–78.
20 M. M. G. Perron, M. Strzelec, M. Gault-Ringold, B. C. Proemse, P. W. Boyd and A. R. Bowie, *Talanta*, 2020, **208**, 120377.
21 G. Cutter, K. Casciotti, P. L. Croot, W. Geibert, L.-E. Heimburger, M. C. Lohan, H. Planquette and T. van de Flierdt, *Sampling and Sample-Handling Protocols for GEOTRACES Cruises*, 2017, vol. 3.
22 G. Rolph, A. Stein and B. Stunder, *Environ. Model. Software*, 2017, **95**, 210–228.
23 S. D. Chambers, S. Preunkert, R. Weller, S.-B. Hong, R. S. Humphries, L. Tositti, H. Angot, M. Legrand, A. G. Williams, A. D. Griffiths, J. Crawford, J. Simmons, T. J. Choi, P. B. Krummel, S. Molloy, Z. Loh, I. Galbally, S. Wilson, O. Magand, F. Sprovieri, N. Pirrone and A. Dommergue, *Front. Earth Sci.*, 2018, **6**, 1–28.
24 R. U. Shelley, P. L. Morton and W. M. Landing, *Deep Sea Res., Part II*, 2015, **116**, 262–272.
25 S. M. McLennan, *Geochem., Geophys., Geosyst.*, 2001, **2**, DOI: 10.1029/2000GC000109.
26 C. L. Mandon, B. W. Christenson, C. I. Schipper, T. M. Seward and E. Garaebiti, *J. Volcanol. Geotherm. Res.*, 2019, **369**, 155–171.
27 G. Menard, S. Moune, I. Vlastélic, F. Aguilera, S. Valade, M. Bontemps and R. González, *J. Volcanol. Geotherm. Res.*, 2014, **287**, 51–67.
28 M. E. Zelenski, T. P. Fischer, J. M. de Moor, B. Marty, L. Zimmermann, D. Ayalew, A. N. Nekrasov and V. K. Karandashev, *Chem. Geol.*, 2013, **357**, 95–116.

29 P. N. Sedwick, E. R. Sholkovitz and T. M. Church, *Geochem., Geophys., Geosyst.*, 2007, **81**, DOI: 10.1029/2007GC001586.
30 S. Byčenkiene, V. Ulevicius, V. Dudoitis and J. Pauraite, *Advances in Meteorology*, 2013, DOI: 10.1155/2013/380614.
31 Global Volcanism Program, in *Report on Heard (Australia)*, ed. S. K. Sennert, Smithsonian Institution and US Geological Survey, 2016.
32 D. Coppola, M. Laiolo, C. Cigolini, F. Massimetti, D. Delle Donne, M. Ripepe, H. Arias, S. Barsotti, C. B. Parra, R. G. Centeno, S. Cevuard, G. Chigna, C. Chun, E. Garaebiti, D. Gonzales, J. Griswold, J. Juarez, L. E. Lara, C. M. López, O. Macedo, C. Mahinda, S. Ogburn, O. Prambada, P. Ramon, D. Ramos, A. Peltier, S. Saunders, E. de Zeeuw-van Dalfsen, N. Varley and R. William, *Front. Earth Sci.*, 2020, **7**, DOI: 10.3389/feart.2019.00362.
33 R. Titelius, *Guardian*, 2016, **1716**(3), https://search.informit.org/doi/10.3316/informit.817600275788628.
34 M. M. G. Perron, B. C. Proemse, M. Strzelec, M. Gault-Ringold, P. W. Boyd, E. S. Rodriguez, B. Paull and A. R. Bowie, *Atmos. Environ.*, 2020, **228**, 117432.
35 A. R. Bowie, D. Lannuzel, T. A. Remenyi, T. Wagener, P. J. Lam, P. W. Boyd, C. Guieu, A. T. Townsend and T. W. Trull, *Global Biogeochem. Cycles*, 2009, **23**(4), DOI: 10.1029/2009GB003500.
36 V. H. Winton, A. R. Bowie, R. Edwards, M. Keywood, A. T. Townsend, P. van der Merwe and A. Bollhöfer, *Mar. Chem.*, 2015, **177**, 20–32.
37 G. Xu and Y. Gao, *Polar Res.*, 2014, **33**, 1–16.
38 Z. Shi, M. D. Krom, T. D. Jickells, S. Bonneville, K. S. K. S. Carslaw, N. Mihalopoulos, A. R. Baker and L. G. Benning, *Aeolian Res.*, 2012, **5**, 21–42.
39 P. Ginoux, J. M. Prospero, T. E. Gill, N. C. Hsu and M. Zhao, *Rev. Geophys.*, 2012, **50**, 1–36.
40 M. L. I. Witt, T. A. Mather, A. R. Baker, J. C. M. De Hoog and D. M. Pyle, *Mar. Chem.*, 2010, **121**, 2–16.
41 E. Journet, K. V. Desboeufs, S. Caquineau and J. L. Colin, *Geophys. Res. Lett.*, 2008, **35**, 1–5.
42 N. M. Mahowald, A. R. Baker, G. Bergametti, N. Brooks, R. A. Duce, T. D. Jickells, N. Kubilay, J. M. Prospero and I. Tegen, *Global Biogeochem. Cycles*, 2005, **19**(4), DOI: 10.1029/2004GB002402.
43 A. Ito, S. Myriokefalitakis, M. Kanakidou, N. M. Mahowald, R. A. Scanza, D. S. Hamilton, A. R. Baker, T. D. Jickells, M. M. Sarin, S. Bikkina, Y. Gao, R. U. Shelley, C. S. Buck, W. M. Landing, A. R. Bowie, M. M. G. Perron, C. Guieu, N. Meskhidze, M. S. Johnson, Y. Feng, J. F. Kok, A. Nenes and R. A. Duce, *Sci. Adv.*, 2019, **5**(5), DOI: 10.1126/sciadv.aau7671.
44 B. Srinivas, M. M. Sarin and A. Kumar, *Biogeochemistry*, 2012, **110**, 257–268.
45 D. S. Mackie, P. W. Boyd, G. H. McTainsh, N. W. Tindale, T. K. Westberry and K. A. Hunter, *Geochem., Geophys., Geosyst.*, 2008, **9**(3), DOI: 10.1029/2007GC001813.
46 E. Sanz Rodriguez, M. M. G. Perron, M. Strzelec, B. C. Proemse, A. R. Bowie and B. Paull, *J. Chromatogr. A*, 2019, **1610**, 460557.
47 J. L. Hand, N. M. Mahowald, Y. Chen, R. L. Siefert, C. Luo, A. Subramaniam and I. Y. Fung, *J. Geophys. Res.*, 2004, **109**(D17), DOI: 10.1029/2004JD004574.
48 S. C. Hsu, G. T. F. Wong, G. C. Gong, F. K. Shiah, Y. T. Huang, S. J. Kao, F. Tsai, S. C. Candice Lung, F. J. Lin, I.-I. Lin, C. C. Hung and C. M. Tseng, *Mar. Chem.*, 2010, **120**, 116–127.
49 A. Heimburger, R. Losno and S. Triquet, *Biogeosciences*, 2013, **10**, 6617–6628.
50 P. Ayris and P. Delmelle, *Phys. Chem. Earth*, 2012, **45–46**, 103–112.
51 A. Heimburger, R. Losno, S. Triquet, F. Dulac and N. M. Mahowald, *Global Biogeochem. Cycles*, 2012, **26**, 1–14.